

## Article

# The Multi-Objective Optimization of Blast Furnace Oxygen Enrichment Rate Based on Optimal Carbon Ratio

Donghui Gao <sup>1,2</sup> , Guoping Luo <sup>1,\*</sup>, Yueming Wang <sup>3</sup> and Guocheng Zhang <sup>4</sup>

<sup>1</sup> School of Materials and Metallurgy, Inner Mongolia University of Science and Technology, Baotou 014010, China

<sup>2</sup> BISG Rare-Earth Steel Iron-Making Plant, Baotou 014010, China

<sup>3</sup> Information Engineering Institute, Inner Mongolia University of Science and Technology, Baotou 014010, China

<sup>4</sup> Department of Chemistry, Baotou Teachers' College, Baotou 014030, China

\* Correspondence: luoguoping3@126.com

**Abstract:** The NSGA-II algorithm was used to establish a multi-objective optimization model for the oxygen enrichment rate of a blast furnace in terms of achieving a lower fuel ratio and higher pulverized coal ratio. The model has the hearth temperature as the constraint condition and the oxygen enrichment rate as the decision variable. The NSGA-II algorithm was used to obtain the Pareto optimal solution of the multi-objective optimization scheme. The prediction effect of the optimization scheme was then tested in industrial experiments. The results show that the optimal setting of the oxygen enrichment rate predicted by the model was 2.70%, which provides an optimal fuel ratio and pulverized coal ratio of 553.86 kg·tHM<sup>-1</sup> and 144.58 kg·tHM<sup>-1</sup>, respectively. In actual production, when the oxygen enrichment rate was set at 2.71%, an optimal fuel ratio and pulverized coal ratio of 553.74 kg·tHM<sup>-1</sup> and 148.73 kg·tHM<sup>-1</sup> were obtained. The relative error in the oxygen enrichment rate between the model prediction and the actual prediction was 0.003%. The prediction results of the model suggest a reduction in CO<sub>2</sub> emissions by 25,770.71 tons per year. The CO<sub>2</sub> emission reduction in actual production was approximately 1.09 times the prediction of the model.

**Keywords:** fuel ratio; pulverized coal ratio; RBF neural network; NSGA-II algorithm; oxygen enrichment rate setting; blast furnace



**Citation:** Gao, D.; Luo, G.; Wang, Y.; Zhang, G. The Multi-Objective Optimization of Blast Furnace Oxygen Enrichment Rate Based on Optimal Carbon Ratio. *Metals* **2023**, *13*, 777. <https://doi.org/10.3390/met13040777>

Academic Editor: Alexander Babich

Received: 21 February 2023

Revised: 9 April 2023

Accepted: 13 April 2023

Published: 15 April 2023



**Copyright:** © 2023 by the authors. Licensee MDPI, Basel, Switzerland. This article is an open access article distributed under the terms and conditions of the Creative Commons Attribution (CC BY) license (<https://creativecommons.org/licenses/by/4.0/>).

## 1. Introduction

Within the iron and steel industry, blast furnace (BF) ironmaking is the process that consumes the most energy and emits the most CO<sub>2</sub> [1–3]. Reducing the fuel ratio (FR) of BF could reduce the smelting cost, energy consumption, and emission of CO<sub>2</sub>. Ren et al. described how oxygen enrichment was an important technical means of BF strengthened smelting and that a high oxygen enrichment rate was beneficial to reducing the FR [4–6]. Yan et al. reported that a high oxygen enrichment rate was beneficial to improving the pulverized coal ratio (PCR) and fuel structure [7,8]. Wu et al. considered that a higher oxygen enrichment rate was beneficial to increasing the production and reducing the energy consumption of BF [9–11]. Maarten Geerdes et al. considered that the best way to reduce greenhouse gas emissions from the blast furnace–BOF route was to use high coal rates and to make use of top gas efficiently [12]. A novel gas–solid suspension ironmaking process with much less energy consumption and carbon dioxide emissions than the current blast furnace technology had been development at the University of Utah. The proposed process would reduce carbon dioxide emissions by 31–35% compared to the average blast furnace process [13]. H. Helle et al. studied the economic advantages and emission reduction effect of using biomass as partial substitute for fossil reductants in the blast furnace (BF) process by simulation [14]. Additionally, with the development of computer technology, industrial big data have become an important technical means to realize the intelligent transformation

and upgrade of the manufacturing industry and have been widely used in industry [15–17]. Li et al. used an intelligent model to predict the burden distribution, pulverized coal injection, parameter adjustment, and silicon content of BF [18–23]. However, there remain unsolved problems. For example, the traditional empirical method was inexperienced with regards to the rational control range of the oxygen enrichment rate, and the effect of oxygen enrichment in reducing the CO<sub>2</sub> emission of BF has not been considered. In blast furnace (BF) production, operators believe that increasing the oxygen enrichment rate was conducive to reducing carbon ratio (CO<sub>2</sub> emissions decreases with reduction of carbon ratio) by traditional experience, but it was lacking in scientific basis to prove it. The paper wants to study the role of oxygen enrichment in reducing CO<sub>2</sub> emissions by the establishment of an intelligent computing model. A new approach for reducing energy use and carbon emissions was proposed for BF. It was important in terms of reducing the carbon peak and achieving carbon neutrality to reduce carbon consumption through oxygen enrichment and thus reducing the CO<sub>2</sub> emission of BF.

This paper determines the target conditions and constraint conditions of the correlation model according to the production demand. By correlation analysis and a RBF neural network prediction model, the main parameters, which affect the target condition and constraint condition functions, were obtained. According to the operation principle of BF, the target condition and constraint condition functions were restricted. Additionally, then the multi-objective genetic algorithm was used to find the oxygen enrichment rate setting when the carbon ratio was optimal, and the CO<sub>2</sub> emissions reduction was calculated according to the carbon ratio. Finally, through industrial tests, the actual effect of CO<sub>2</sub> emissions to reduce oxygen enrichment was examined.

## 2. Data Processing and Correlation Analysis

The parameters of a BF were stable and continuous in normal operation. It was, therefore, reasonable to use distribution-based outlier screening methods to process model data, and the Pauta criterion ( $3\sigma$  criterium) [24] was usually used in screening out distribution-based outliers. One year of production data for a 4150 m<sup>3</sup> BF operated by Baotou Steel were collected, and, from these data, 270 sets were selected for modeling calculations after data screening and repair using the Pauta criterion. Spearman's correlation coefficient [25] was used to reduce the data dimensionality and, thus, the difficulty of model calculation in an analysis of linear association of the input variable and output variable. A radial basis function (RBF) neural network [26] was used to establish a correlation model with the FR and PCR of BF as optimization objectives, the hearth temperature as the constraint condition, and the oxygen enrichment rate as the decision variable. The multi-objective optimization of the model prediction results, based on the NSGA-II algorithm [27,28], was then performed to obtain the Pareto optimal solution of the setting of the oxygen enrichment rate.

### 2.1. Outlier Screening of the Production Data

The data that, according to the Pauta criterion, were missing or deviated from the average arithmetical mean of the sample by more than  $3\sigma$  were considered abnormal data. The standard deviation  $\sigma$  of the sample data was calculated as

$$\sigma = \sqrt{\frac{1}{n} \sum_{i=1}^n (x_i - \mu)^2}, \quad (1)$$

where  $x_i$  denotes the sample data, and  $\mu$  was the average value of the sample data.

Abnormal data were assigned a null value. The average arithmetical mean of the four data before and four data after the null value were considered, which was used in place of the abnormal datum in repairing the data.

## 2.2. Analysis of the Linear Association of the Production Parameter

The use of all 16 input variables and four output variables in modeling would have a high calculation cost and high complexity. Spearman's algorithm was thus used to calculate Spearman's coefficient of correlation between the input variables and output variables to reduce the data dimension and computational cost. Spearman's correlation coefficient  $\rho$  was calculated as

$$\rho = \frac{\sum_i (x_i - \bar{x})(y_i - \bar{y})}{\sqrt{\sum_i (x_i - \bar{x})^2 \sum_i (y_i - \bar{y})^2}}, \quad (2)$$

where  $x_i$  and  $y_i$ , respectively, denote the samples of input variables and output variables, and  $\bar{x}$ , and  $\bar{y}$  were, respectively, the mean values of the input and output variables.

The calculation results were given in Table 1. The modeling treats data with  $|\rho| \geq 0.15$  as variables with good correlation and uses them as key variables in the correlation model.

**Table 1.** Spearman's rank correlation coefficient.

Parameter Name	FR ( $f_1$ )	PCR ( $f_2$ )	Hot Metal Temperature ( $g_1$ )	Hot Metal Silicon Content ( $g_2$ )
Charging rate ( $m_1$ )	-0.45	0.28	0.13	-0.15
Blast volume ( $m_2$ )	-0.28	0.49	-0.02	-0.36
Hot blast pressure ( $m_3$ )	-0.10	0.60	0.30	0.12
Top pressure ( $m_4$ )	-0.16	0.67	0.14	-0.03
Pressure difference ( $m_5$ )	0.06	0.05	0.32	0.24
Air permeability resistance index ( $m_6$ )	0.21	-0.49	-0.02	0.20
Blast temperature ( $m_7$ )	0.14	0.59	0.13	0.00
Oxygen enriched rate ( $m_8$ )	0.20	0.44	0.19	0.20
Coke rate ( $m_9$ )	0.41	-0.74	-0.27	0.03
Water temperature drop ( $m_{10}$ )	0.31	-0.06	-0.10	0.07
Gas utilization efficiency ( $m_{11}$ )	-0.67	-0.02	0.16	0.04
(n - 1) Hot metal temperature ( $n_1$ )	-0.06	0.29	0.10	-0.11
(n - 1) Hot metal silicon content ( $n_2$ )	0.27	0.40	-0.05	-0.02
(n - 1) Hot metal manganese content ( $n_3$ )	0.05	0.17	-0.08	-0.22
(n - 1) Hot metal phosphorus content ( $n_4$ )	0.06	0.41	0.05	-0.05
(n - 1) Hot metal sulfur content ( $n_5$ )	-0.25	0.27	0.27	0.12

Table 1 shows that there were 9 variables having better correlation with the FR  $f_1$ , namely,  $m_1, m_2, m_4, m_6, m_8, m_9, m_{10}, n_2$ , and  $n_5$ , 13 variables having better correlation with the PCR  $f_2$ , namely,  $m_1, m_2, m_3, m_4, m_6, m_7, m_8, m_9, n_1, n_2, n_3, n_4$ , and  $n_5$ , five variables having better correlation with the hot metal temperature  $g_1$ , namely,  $m_3, m_5, m_8, m_9$ , and  $n_5$ , and six variables having better correlation with the hot metal silicon  $g_2$ , namely,  $m_1, m_2, m_5, m_6, m_8$ , and  $n_3$ . Further screening through model testing was required, and then the optimal variable from the above variables was selected to establish a correlation model.

## 3. The Creation and Analysis of Correlation Model

### 3.1. RBF Neural Network Algorithm Principle

The RBF neural network [29] was a three-layer forward neural network. The network performs well in approximating nonlinear functions. The hidden layer was nonlinear. The input layer vector space was converted to the hidden layer space using a RBF. Through converting the original linear inseparable problem into a linear separable problem, a linear output was obtained from the output layer.

(1) The basis function of the RBF hidden layer was:

$$\Phi_i(X_p) = \exp\left(-\frac{\|X_p - c_i\|_2^2}{2\sigma_i^2}\right), \quad (3)$$

where  $i = 1, 2, 3, \dots, m, p = 1, 2, 3, \dots, n, r$  was the number of nodes in the hidden layer,  $c_i$  was the  $i$ th node center of the hidden layer,  $\sigma$  was a shape parameter of the  $i$ th center vector, and  $\|X_p - c_i\|_2$  was a characterization of the Euclidean distance between  $X_p$  and  $c_i$ .

(2) The basis function of the RBF output layer was:

$$y_i = b_j + \sum_{i=1}^r w_{ij} \phi_i(X_p), \quad (4)$$

where  $j = 1, 2, 3, \dots, s, w_{ij}$  denotes the output layer weights, and  $b_j$  was the threshold of the output layer.

### 3.2. Construction and Analysis of the Correlation Model

#### (1) Constraint condition modeling

In BF production, the suitability of the FR and PCR were often measured in terms of the hearth temperature. A higher FR and PCR correspond to more heat generated and a higher hearth temperature, whereas a lower FR and PCR corresponds to less heat generated and a lower furnace temperature. There were two ways of measuring the hearth temperature, namely, by measuring hot metal temperature and hot metal silicon content. The RBF neural network based on time series was used to establish the correlation model of hot metal temperature and hot metal silicon content. The model structure was then debugged according to the consistency between the predicted value and actual value. Finally, four variables, namely, the pressure difference ( $m_5$ ), oxygen enrichment rate ( $m_8$ ), sulfur content of the previous furnace ( $n_5$ ), and hot blast pressure ( $m_3$ ), were selected as input variables in establishing the correlation model of the hot metal temperature. Five variables, namely, the pressure difference ( $m_5$ ), oxygen enrichment rate ( $m_8$ ), charging rate ( $m_1$ ), blast volume ( $m_2$ ), and manganese content of the previous hot metal ( $n_3$ ), were selected as input variables in establishing the silicon content correlation model. Following parameter optimization, the correlation model of the hot metal temperature and silicon content had 22 and 26 clustering centers respectively and better accuracy. The prediction curve was shown in Figure 1. Introducing production experience, the correlation model of the hot metal temperature and silicon content based on the RBF network were established as

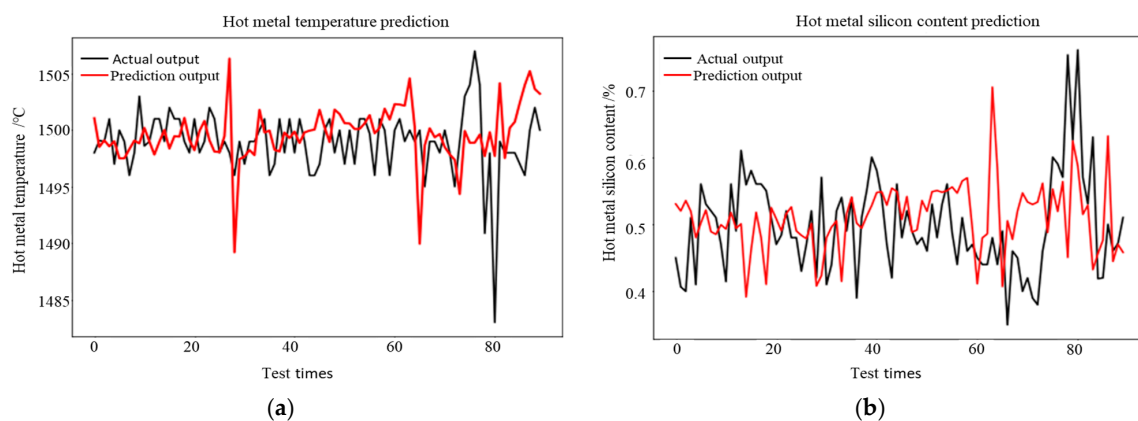


**Figure 1.** Hot metal temperature and silicon content correlation model: (a) comparison between the model prediction and actual hot metal temperature and (b) comparison between the model prediction and actual hot metal silicon content.

$$\begin{cases} g_1(m_5, m_8, n_5, m_3) = b_1 + \sum_{i=1}^{N_1} w_{i1} \phi_i(X_p) \\ g_2(m_5, m_8, m_2, n_3, m_1) = b_2 + \sum_{i=1}^{N_2} w_{i2} \phi_i(X_p) \end{cases} \quad (5)$$

Model predictions for the temperature and silicon content of the hot metal were shown in Figure 1. The predicted output of the model was consistent with the actual output. The relative error between the prediction output of the temperature correlation model and actual output was 0.002%, whereas the relative error between the prediction output of the silicon content correlation model and actual output was 0.13%, and the relative errors were all less than 5%, showing that the correlation models perform well.

## (2) Target condition modeling

Combined with production practice, the RBF neural network, based on K-means clustering, was used to establish the correlation model of FR and PCR with oxygen enrichment rate (Conversion among CR, PCR, and FR was  $CR = FR - PCR$ , and the value of CR can be determined by PCR and FR. Therefore, this paper chooses PCR and FR for modeling. CR can also be used to replace PCR for modeling). After debugging the model structure, according to the consistency between predictions and actual values, five variables, namely, the charging rate ( $m_1$ ), silicon content of the previous hot metal ( $n_2$ ), sulfur content of the previous hot metal ( $n_5$ ), top pressure ( $m_4$ ), and oxygen enrichment rate ( $m_8$ ), were selected as input variables in establishing the FR correlation model. Six variables, namely, the oxygen enrichment rate ( $m_8$ ), manganese content of the previous hot metal ( $n_3$ ), sulfur content of the previous hot metal ( $n_5$ ), top pressure ( $m_4$ ), hot blast pressure ( $m_3$ ), and air permeability resistance index ( $m_6$ ), were selected as input variables in establishing the PCR correlation model of the hot metal. Following parameter optimization, the correlation models of the FR and PCR had 18 and 22 clustering centers, respectively, and better accuracy. The prediction curve was shown in Figure 2. Through introducing production experience, correlation models of the FR and PCR based on the RBF network were established as

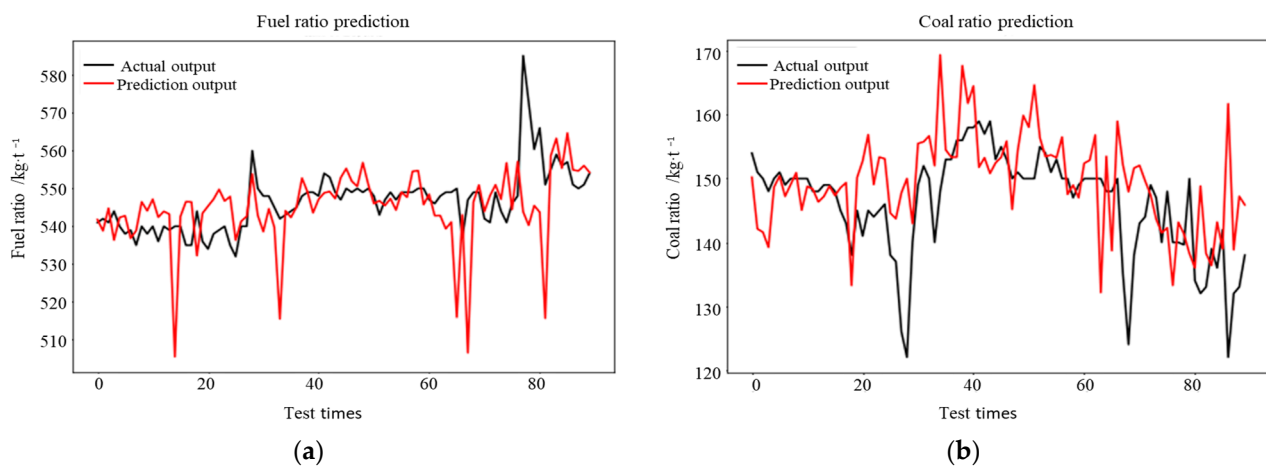


**Figure 2.** FR and PCR correlation model: (a) comparison between the model prediction and actual FR and (b) comparison between the model prediction and actual PCR.

$$\begin{cases} f_1(m_1, n_2, n_5, m_4, m_8) = b_3 + \sum_{i=1}^{N_3} w_{i3} \phi_i(X_p) \\ f_2(m_8, n_3, m_4, m_3, m_6, n_5) = b_4 + \sum_{i=1}^{N_4} w_{i3} \phi_i(X_p) \end{cases} \quad (6)$$

Model predictions for the FR and PCR were shown in Figure 2. The prediction output of the model was consistent with the actual output. The relative error between the prediction output of the FR correlation model and the actual output was 0.01%, whereas the relative error between the prediction output of the PCR correlation model and the actual output was 0.05%. The relative errors were all less than 5%, showing that the correlation models perform well.

The absolute error, relative error, and hit rate of the correlation model were used to verify the performance of the correlation model, as shown in Table 2.

**Table 2.** Evaluation indicators for model.

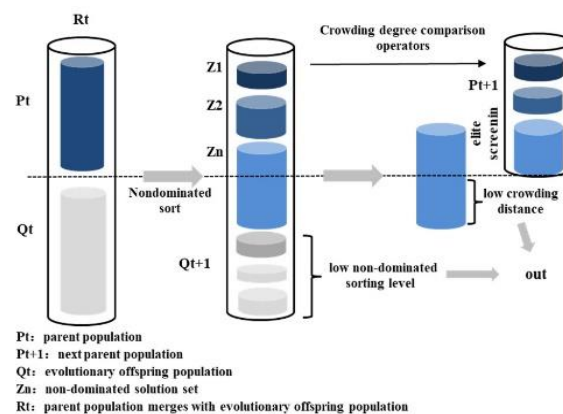
Parameter Name	FR/kg·t <sup>-1</sup>	PCR/kg·t <sup>-1</sup>	Hot Metal Temperature/°C	Hot Metal Silicon Content/%
Absolute error	3.28	1.57	0.84	0.03
Relative error /%	0.01	0.05	0.002	0.13
Hit rate /%	90.00	70.00	100.00	73.33

Table 2 shows that the relative error and hit rate of the model predictions were within a reasonable control range. The FR and hot metal temperature models had high hit rates of 90.00% and 100.00% and low relative errors of 0.01% and 0.002%, respectively, showing their excellent performance. The PCR and hot metal silicon content models had hit rates of 70.00% and 73.33% and relative errors of 0.05% and 0.13%, respectively, showing their good performance. The absolute error in the prediction of the hot metal temperature model was 0.85 °C, the absolute error in the prediction of the hot metal silicon content model was 0.03%, the absolute error in the prediction of the PCR model was 1.62 kg·tHM<sup>-1</sup>, and the absolute error in the prediction of the FR model was 0.53 kg·tHM<sup>-1</sup>. The absolute errors show good prediction performance of the constraint condition and target condition modeling. Additionally, owing to the effect of BF blowing-down and abnormal furnace condition, some predictions deviated from actual situation. If the relevant data were taken as outliers to supplement or correct, although the consistency of the prediction can be improved, there was an increase in the difference between the model prediction and the actual situation, which reduces the accuracy of the subsequent multi-objective optimization calculation. Therefore, to fit well with the actual situation, it was necessary to consider reducing the hit rate of the correlation model appropriately, as well as not supplementing or correcting the data of the blowing-down and abnormal furnace conditions.

#### 4. Correlation Model Optimization Based on the NSGA-II Multi-Objective Genetic Algorithm

##### 4.1. Principle of NSGA-II Multi-Objective Genetic Algorithm

The elite strategy was introduced into the NSGA-II algorithm [30]. The method of nondominated sorting mixed the excellent population of the father generation with its offspring to effectively avoid the loss of excellent individuals in the parent population and to ensure the superiority of next-generation fathers. The execution steps of the elite strategy were presented in Figure 3.



**Figure 3.** Execution steps of the elite strategy.

The algorithm flow was as follows.

- (1) Combine the evolutionary offspring population ( $Q_t$ ) with the parent population ( $P_t$ ) to constitute populations ( $R_t$ ) with a size of  $2N$ . Then, sort the population ( $R_t$ ) in a nondominated manner to find a series of nondominated sets ( $Z_1$ ) and calculate the crowding degree of each individual.
- (2)  $Z_1$  was the optimal individual set with high rank and large aggregation distance for the overall  $R_t$  population. Put  $Z_1$  in the new parent population  $P_{t+1}$ .
- (3) If the  $P_{t+1}$  population was smaller than  $N$ , then the next nondominated set  $Z_2$  needs to be added to  $P_{t+1}$  until  $Z_n$  was added to the nondominated set and the population exceeds  $N$ . The crowding comparison operator was then used for each individual in  $Z_n$ . Take the previous  $\{\text{num}(Z_n) - (\text{num}(P_{t+1}) - N)\}$  individuals so that the size of the  $P_{t+1}$  population reaches  $N$ .
- (4) Through genetic operators, such as selection, crossover, and mutation, the next parent  $P_{t+1}$  generates a new offspring population  $Q_{t+1}$ .
- (5) The next parent  $P_{t+1}$  produces a new offspring population  $Q_{t+1}$  and merges it into a new population  $R_{t+1}$ . The nondominated population was then reordered.
- (6) Repeat steps (1)~(5) until the evolutionary algebra reaches the maximum evolutionary algebra  $Gen_{max}$ . The final parent population was the optimal solution set of the problem.

#### 4.2. Multi-Objective Optimization Results and Analysis of the NSGA-II Algorithm

Multi-objective optimization: the oxygen enrichment rate was used as a decision variable in the optimization process, and the temperature and silicon content of the hot metal were used as constraint conditions. Following BF operational experience, when the reasonable range of the hot metal temperature was controlled at 1490–1510 °C, the silicon content of the hot metal was controlled at 0.45–0.55%, and it was possible to maintain low fuel consumption while keeping BF operation smooth. Otherwise, when adjusting the order of variables of the model according to production experience, the reasonable constraint range of the oxygen enrichment rate in decision variables was 1–4%. The multi-objective optimization model was expressed as:

$$\left\{ \begin{array}{l} \min f_1(m_1, n_5, n_2, m_4, m_8) \\ \max f_2(m_8, n_3, m_4, m_3, m_6, n_5) \\ 1490 < g_1(m_5, m_8, n_5, m_3) < 1510 \\ 0.45\% < g_2(m_5, m_8, m_1, m_2, n_3) < 0.55\% \\ 1\% < m_8 < 4\% \end{array} \right. \quad (7)$$

The model population size was set at 90, the maximum evolutionary algebra was set at 200, and the Pareto front curve obtained by solving decision variables was shown in Figure 4. The abscissa  $F_1$  was the FR, and the ordinate  $F_2$  was the PCR.

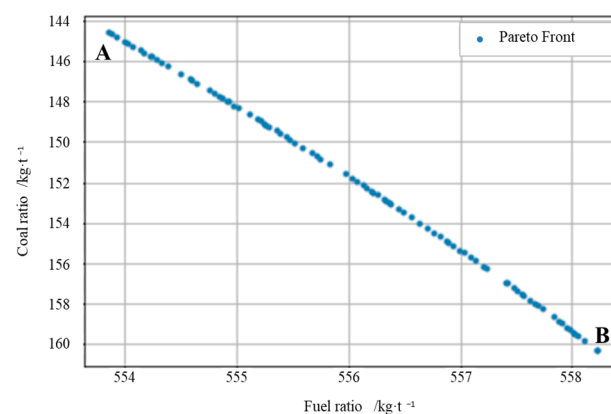


**Figure 4.** Pareto optimal front curve of the multi-objective optimization model. (Point A and B were the two endpoints of the curve).

The Pareto front curve of the multi-objective optimization model shown in Figure 4 reveals that the FR was lower, but the coal ratio was higher at point A, whereas the FR was higher, but the coal ratio was lower at point B. According to production experience, the most reasonable scheme for improving the carbon ratio was ensuring a lower FR. Therefore, the lower FR values of three points close to point A on the Pareto front curve were selected as the optimal solution set, as shown in Table 3.

**Table 3.** Multi-objective optimization results.

Variable Name	Current Level	Multi-Objective Optimization Value 1	Multi-Objective Optimization Value 2	Multi-Objective Optimization Value 3
Oxygen enriched rate/%	2.81	2.70	2.72	2.71
Hot metal temperature/°C	1500.00	1503.52	1503.47	1503.50
Hot metal silicon content/%	0.51	0.45	0.45	0.45
FR/kg·t <sup>-1</sup>	555.21	553.86	553.92	553.88
PCR/kg·t <sup>-1</sup>	133.10	144.58	144.78	144.63
CR/kg·t <sup>-1</sup>	422.11	409.28	409.15	409.25

Table 3 shows that, among the three optimal solutions, the ideal FR and PCR can be obtained under the constraint condition of a suitable hearth temperature. In the first solution set, the FR was greatly reduced, and the PCR was high. According to production experience, when the utilization of gas ( $\eta_{CO}$ ) in the first solution set was 44%, the oxygen enrichment rate was 2.70%, the optimal FR was 553.86 kg·tHM<sup>-1</sup>, and hearth temperature index was at a suitable level. The model FR was 1.35 kg·tHM<sup>-1</sup> lower than the current FR of 555.21 kg·tHM<sup>-1</sup>, and the model PCR was 6.58 kg·tHM<sup>-1</sup> higher than the current PCR of 133.10 kg·tHM<sup>-1</sup>.

The value of calculation parameters: the effective volume of BF was 4150 m<sup>3</sup>, the average utilization coefficient was 2.11 t·m<sup>-3</sup>·d<sup>-1</sup> (consider the effect of blowing-down), the average carbon content of the fuel was 81.33%, carbon atoms have a molar mass of 12 g·mol<sup>-1</sup>, oxygen atoms have a molar mass of 16 g·mol<sup>-1</sup>, and CO<sub>2</sub> emissions were expected to reduce by 25,770.71 ton per year. The calculation was written as:

$$2.11 \times 4150 \times 2 \times 365 \times 1.35 \times 10^{-3} \times 81.33\% \times \frac{44}{12} = 25,770.71(\text{t/a}). \quad (8)$$

## 5. Application and Analysis of the Multi-Objective Optimization Results

### 5.1. Industrial Test of Multi-Objective Optimization Results

To verify the prediction of the model, 146 industrial tests were carried out on a 4150 m<sup>3</sup> BF at Baotou Steel. Changes in the FR and PCR at different oxygen enrichment rates were shown in Figure 5. It was difficult to obtain the relationship between the FR and PCR and oxygen enrichment rate in Figure 5. Therefore, the FR and PCR were first converted into index K and then compared. The hearth temperature and gas utilization rate corresponding to the FR and PCR in the industrial test data in Figure 5 were different. Before calculating the K value, it was necessary to convert the FR and PCR data in Figure 5 to under the same silicon content and gas utilization rate condition.

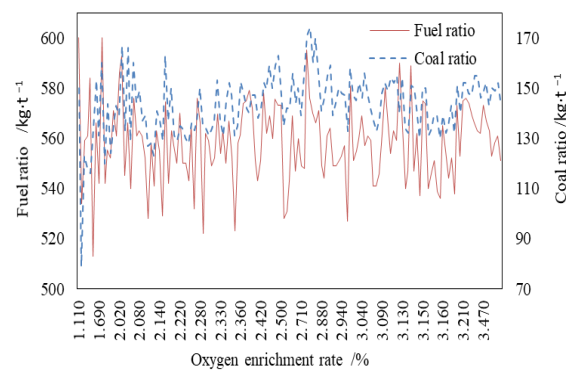


**Figure 5.** Results of the industrial test.

Let the ratio of FR to PCR be K, the K was calculated as:

$$K = Fr/PCR \quad (9)$$

Equation (9) shows that smaller K corresponds to a better fuel structure of BF, lower carbon consumption, and lower CO<sub>2</sub> emissions. According to the production experience for BF [2], the FR increases approximately 5.00 kg·tHM<sup>-1</sup> for every 0.10% increase in the silicon content of the hot metal, and the FR decreases by approximately 5.00 kg·tHM<sup>-1</sup> for every 1.00% increase in η<sub>CO</sub>. From the 146 groups of experimental data in Figure 6, 37 groups of data with the smallest K value (approximately 25% of the data size) were selected, and the average oxygen enrichment rate of the group and the arithmetic average value of K were used as the optimal solution in the industrial data. The results show that when the average oxygen enrichment rate was 2.71%, the average K value was 3.72, the carbon consumption of BF was lowest, the average FR was 553.74 kg·tHM<sup>-1</sup>, and the average PCR was 148.73 kg·tHM<sup>-1</sup>. The relative error between the optimal oxygen enrichment value predicted by the model and the measured value obtained in the industrial test was 0.01%. This small error was considered to be a measurement error. The measurement error of the oxygen meter was ±0.50%. The FR in the industrial test was 1.47 kg·tHM<sup>-1</sup> lower than the current FR of 555.21 kg·tHM<sup>-1</sup>, whereas the PCR in industrial tests was 10.73 kg·tHM<sup>-1</sup> higher than the current PCR of 133.10 kg·tHM<sup>-1</sup>. CO<sub>2</sub> emissions were expected to decrease by 28,137.80 tons per year. The calculation was written as:

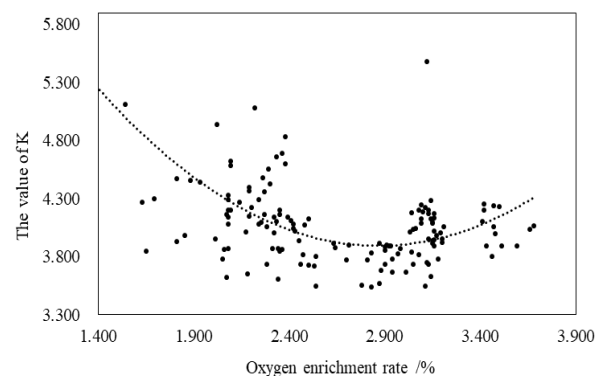


**Figure 6.** Effect of K for different oxygen enrichment rates.

$$2.11 \times 4150 \times 2 \times 365 \times 1.47 \times 10^{-3} \times 81.33\% \times \frac{44}{12} = 28,137.80(\text{t/a}). \quad (10)$$

The CO<sub>2</sub> emission reduction was approximately 1.09 times that predicted by the model.

## 5.2. Analysis of Industrial Test Results

In the multi-objective optimization model of the NSGA-II algorithm based on the correlation model, the Pareto optimal solution set for multi-objective optimization needs to be determined by considering both the carbon consumption and carbon consumption structure so as to determine the final optimization results. The trend of the curve in Figure 6 shows that, under the present smelting conditions at Baotou Steel, when the oxygen enrichment rate was controlled within a certain range, the FR decreases with an increase in the oxygen enrichment rate, the reason being that, with an increase in the oxygen enrichment rate, the CO concentration of BF gas increases, which was conducive to indirect reduction, the energy utilization rate increases, and little carbon was consumed. At this time, FR was low, and the structure of carbon consumption was reasonable, and the CO<sub>2</sub> emission was reduced. However, when the oxygen enrichment rate increases beyond a certain range, the FR increases with an increase in the oxygen enrichment rate, the reason being that, with an increase in the oxygen enrichment rate, the consumption rate of burden was accelerated, and its residence time in indirect reduction zone was shortened. Additionally, the increase in oxygen enrichment will limit the increase in blast volume, and the physical heat brought into the BF by the blast was relatively reduced, which will eventually weaken the heating and reduction of the furnace burden. At this time, FR was high, and the CO<sub>2</sub> emission was increased.

The calculation results of the multi-objective optimization model were consistent with the industrial test results. The coincidence rate of the oxygen enrichment rate was 99.67%, whereas the coincidence rate of the optimal FR was 99.98%. Figure 6 shows that too high or too low oxygen enrichment leads to higher FR, and only by controlling the oxygen enrichment rate within a certain range can FR be reduced. Carbon emissions also decrease with the decrease in FR. The predicted effect of the optimization scheme obtained by the model calculation was consistent with the practical application effect. This provides a new research direction for the carbon reduction and emission reduction of super BFs, and the approach can be adopted in related research on the same grade of BF and super BFs.

## 6. Conclusions

The model calculation results show that, when the multi-objective optimization value of the oxygen enrichment rate was 2.70%, the optimal carbon ratio were obtained. On the basis of the multi-objective optimization oxygen enrichment rate, it was expected that the FR can be reduced by 1.35 kg·tHM<sup>-1</sup>, and CO<sub>2</sub> emissions can be reduced by 25,770.71 tons per year. The industrial tests show that, when the oxygen enrichment rate was set close to optimal result, the FR can be reduced by 1.47 kg·tHM<sup>-1</sup>, and the annual CO<sub>2</sub> emission can be reduced by 28,137.80 tons. The effect of the CO<sub>2</sub> emission reduction in BF production was 1.09 times that in the model prediction. The relative error between the optimal oxygen enrichment rate obtained by multi-objective optimization, and the industrial test result was 0.003%, whereas that for the fuel ratio was 0.02%. The multi-objective optimization model prediction was consistent with the industrial test results. The goal of reducing carbon ratio and CO<sub>2</sub> emissions can thus be achieved by setting a reasonable oxygen enrichment rate.

In addition, industrial test results show that it was very different from traditional experience. A higher or lower oxygen enrichment rate leads to higher carbon ratios, and only by controlling the oxygen enrichment rate within a certain range can the enrichment rate play a role in reducing carbon ratio. For the existing smelting conditions of a BF at Baotou Steel, the setting of a reasonable oxygen enrichment rate can improve the fuel structure, save energy, and reduce CO<sub>2</sub> emissions.

**Author Contributions:** Conceptualization, D.G.; methodology, D.G.; software, Y.W.; resources, D.G. and G.L.; writing—original draft, D.G.; writing—review & editing, D.G., G.L. and G.Z. All authors have read and agreed to the published version of the manuscript.

**Funding:** This research received no external funding.

**Institutional Review Board Statement:** Not applicable.

**Informed Consent Statement:** Not applicable.

**Data Availability Statement:** Data is unavailable due to privacy restrictions.

**Conflicts of Interest:** The authors declare no conflict of interest.

## References

1. Zhou, D.; Cheng, S.; Wang, Y.; Jiang, X. The production of large blast furnaces during 2016 and future development of ironmaking in China. *Ironmak. Steelmak.* **2017**, *44*, 714–720. [[CrossRef](#)]
2. Zhou, C.D. *Technical Manual of Blast Furnace Iron-Making Production*; Metallurgical Industry Press: Beijing, China, 2002; pp. 367–368.
3. Zhang, F.M.; Cao, C.Z.; Meng, X.L.; Li, L. Technological Development Orientation on Ironmaking of Contemporary Blast Furnace. *Adv. Mater. Res.* **2014**, *2949*, 1138–1142. [[CrossRef](#)]
4. Ren, L.J.; Wei, H.Q. Practice on intensified smelting and target output achievement in No.1 BF of ShoufangJingtang joint Co., Ltd. *Ironmaking* **2010**, *29*, 16–19.
5. Wakabayashi, K.; Fujiura, M.; Mori, T.; Inoue, N. Theoretical Analyses on the High Top-Gas-Pressure Operation and Oxygen-Enriched Operation of Blast Furnace. *Trans. Iron Steel Inst. Jpn.* **1970**, *10*, 207–215. [[CrossRef](#)]
6. Xiang, Z.Y.; Zhu, R.L. Reducing Fule Ratio While Increasing Oxygen Enrichment to Enhance Blast Furnace Output. *Iron Steel* **2010**, *45*, 9–12+17. [[CrossRef](#)]
7. Yan, C.J.; Cheng, X.L.; Gao, J.J.; Zhou, Y.S. Effect of High Oxygen Enrichment PCI on BF Iron-Making. *Iron Steel* **2013**, *48*, 25–28. [[CrossRef](#)]
8. Wang, G.W.; Zhang, J.L.; Shao, J.G. Model for Economic Evaluation of Iron Production With Oxygen-Enriched and Pulverized Coal Injection. *Iron Steel* **2013**, *48*, 21–26. [[CrossRef](#)]
9. Wu, L.Y.; Hu, L.H.; Wang, W.Y. Contribution of high oxygen enrichment rate to energy saving for large blast furnace. *Energy Metall. Ind.* **2020**, *39*, 18–20+54.
10. Zhang, J.; Wang, K.; Wang, Z. Matching analysis of oxygen enrichment rate with furnace condition of No.1 blast furnace in ShoufangJingtang. *J. Iron Steel Res.* **2020**, *32*, 720–726. [[CrossRef](#)]
11. Yu, X.B.; Ni, W.J.; Zou, Z.S. Integrated Model of Oxygen-Enriched Blast Furnace. *J. North. Univ. (Nat. Sci.)* **2018**, *39*, 1248–1252+1314.
12. Geerdes, M.; Chaigneau, R.; Lingardi, O. *Modern Blast Furnace Ironmaking*; Delft University Press: Delft, The Netherlands, 2015; pp. 188–189.
13. Pinegar, H.K.; Moats, M.S.; Sohn, H.Y. Flowsheet development, process simulation and economic feasibility analysis for novel suspension iron-making technology based on natural gas. *Ironmak. Steelmak.* **2013**, *40*, 32–43. [[CrossRef](#)]
14. Helle, H.; Helle, M.; Pettersson, F.; Saxén, H. Optimisation study of ironmaking using biomass. *Ironmak. Steelmak.* **2010**, *37*, 590–598. [[CrossRef](#)]
15. Wei, M.; Wang, Q.; Ye, M.; Li, J.B.; Xu, X.X. An indirect remaining useful life prediction of lithium-ion batteries based on a NARX dynamic neural network. *Chin. J. Eng.* **2022**, *44*, 380–388. [[CrossRef](#)]
16. Liu, H.L.; Wu, S.; Wei, G.Y.; Li, X.; Gao, X.N. Click-through rate prediction model based on a deep neural network. *Chin. J. Eng.* **2022**, *44*, 1917–1925. [[CrossRef](#)]
17. Liu, S.; Wang, X.D.; Wu, N. A CNN-based CSI fingerprint indoor localization method. *Sci. Technol. Eng.* **2021**, *43*, 1512–1521. [[CrossRef](#)]
18. Pei, Y.Y.; Yang, X.B.; Chuan, J.P.; Wu, X.S.; Cheng, H.M.; Lv, X.F. Time series prediction of microseismic energy level based on feature extraction of one-dimensional convolutional neural network. *Sci. Technol. Eng.* **2021**, *43*, 1003–1009. [[CrossRef](#)]
19. Cui, G.M.; Lv, M.Y. Multi-objective optimization of furnace coal injection setting based on optimal fuel ratio. *Sci. Technol. Eng.* **2020**, *20*, 4022–4028.
20. Park, J.I.; Jung, H.J.; Jo, M.K.; Oh, H.-S.; Han, J.-W. Mathematical modeling of the burden distribution in the blast furnace shaft. *Met. Mater. Int.* **2011**, *17*, 485–496. [[CrossRef](#)]
21. Li, Z.N.; Chu, N.S.; Liu, Z.G.; Li, B.F. Prediction and optimization of blast furnace parameters based on machine learning and genetic algorithm. *J. North. Univ. (Nat. Sci.)* **2020**, *41*, 1262–1267.
22. Hua, C.; Wu, J.; Li, J.; Guan, X. Silicon content prediction and industrial analysis on blast furnace using support vector regression combined with clustering algorithms. *Neural Comput. Appl.* **2017**, *28*, 4111–4121. [[CrossRef](#)]
23. Fahmideh, M.; Beydoun, G. Big data analytics architecture design-An application in manufacturing systems—Science Direct. *Comput. Ind. Eng.* **2019**, *128*, 948–963. [[CrossRef](#)]
24. Chen, S.; Cowan, C.N.; Grant, P.M. Orthogonal least squares learning algorithm for radial basis function networks. *IEEE Trans. Neural Netw.* **1991**, *2*, 302–309. [[CrossRef](#)] [[PubMed](#)]
25. Xiao, M.Y. How to eliminate observations containing gross errors. *Metrol. Sci. Technol.* **1973**, *2*, 13–15.
26. Sedgwick, P. Spearman's rank correlation coefficient. *BMJ* **2018**, *362*, k4131. [[CrossRef](#)] [[PubMed](#)]
27. Liu, S. *Python Machine Learning Algorithm Principle, Implementation and Case Study*; Tsinghua University Publishing: Beijing, China, 2019; pp. 184–196.

28. Chen, X.Q.; Hou, Z.X.; Guo, L.M.; Luo, W.C. Improved multi-objective genetic algorithm based on NSGA-II. *J. Comput. Appl.* **2006**, *26*, 2453–2456.
29. Niu, Z.J. *The Application Research on Prediction and Classification Based on Artificial Neural Network*; North University of China: Taiyuan, China, 2016; pp. 2–13.
30. Deb, K.; Pratap, A.; Agarwal, S.; Meyarivan, T.A.M.T. A fast and elitist multi-objective genetic algorithm: NSGA-II. *IEEE Trans. Evol. Comput.* **2002**, *6*, 182–197. [[CrossRef](#)]

**Disclaimer/Publisher’s Note:** The statements, opinions and data contained in all publications are solely those of the individual author(s) and contributor(s) and not of MDPI and/or the editor(s). MDPI and/or the editor(s) disclaim responsibility for any injury to people or property resulting from any ideas, methods, instructions or products referred to in the content.